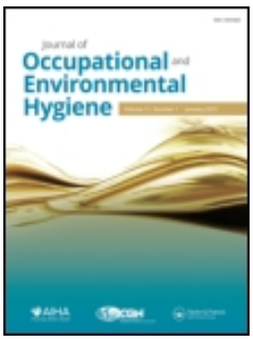

Journal of Occupational and Environmental Hygiene

ISSN: 1545-9624 (Print) 1545-9632 (Online) Journal homepage: http://www.tandfonline.com/loi/uoeh20

Modeling the Wet Bulb Globe Temperature Using Standard Meteorological Measurements

James C. Liljegren , Richard A. Carhart , Philip Lawday , Stephen Tschopp & Robert Sharp

To cite this article: James C. Liljegren , Richard A. Carhart , Philip Lawday , Stephen Tschopp & Robert Sharp (2008) Modeling the Wet Bulb Globe Temperature Using Standard Meteorological Measurements, Journal of Occupational and Environmental Hygiene, 5:10, 645-655, DOI: 10.1080/15459620802310770

To link to this article: https://doi.org/10.1080/15459620802310770

Published online: 04 Aug 2008.

Journal of Occupational and Environmental Hygiene, 5: 645–655
ISSN: 1545-9624 print / 1545-9632 online

DOI: 10.1080/15459620802310770

Modeling the Wet Bulb Globe Temperature Using Standard Meteorological Measurements

James C. Liljegren, Richard A. Carhart, Philip Lawday, Stephen Tschopp, and Robert Sharp

Argonne National Laboratory, Decision and Information Sciences Division, Lemont, Illinois

The U.S. Army has a need for continuous, accurate estimates of the wet bulb globe temperature to protect soldiers and civilian workers from heat-related injuries, including those involved in the storage and destruction of aging chemical munitions at depots across the United States. At these depots, workers must don protective clothing that increases their risk of heat-related injury. Because of the difficulty in making continuous, accurate measurements of wet bulb globe temperature outdoors, the authors have developed a model of the wet bulb globe temperature that relies only on standard meteorological data available at each storage depot for input. The model is composed of separate submodels of the natural wet bulb and globe temperatures that are based on fundamental principles of heat and mass transfer, has no site-dependent parameters, and achieves an accuracy of better than 1°C based on comparisons with wet bulb globe temperature measurements at all depots.

Keywords environmental measurements, heat indexes, heat stress

Address correspondence to: James C. Liljegren, Decision and Information Sciences Division, Argonne National Laboratory, 9700 South Cass Avenue, Lemont, IL 60439-4832; e-mail: jcliljegren@anl.gov.

INTRODUCTION

The wet bulb globe temperature (WBGT) is used by the U.S. Occupational Safety and Health Administration (OSHA)[1] and the U.S. Army[2] for identifying environmental conditions under which individuals are likely to experience heat stress effects and for implementing protective controls to prevent heat-related injuries. The U.S. Army has a need to protect soldiers and civilian employees, including those involved in the storage and destruction of aging chemical munitions, during outdoor activities at seven depots across the United States. At these depots workers must don protective clothing that increases their risk of heat-related injury.

OSHA heat stress guidelines[1] include adjustments to the WBGT to account for several types of work clothing. According to the U.S. Army work/rest guidelines[2] for warm weather training conditions, if mission-oriented protective posture (MOPP) level 4 clothing is worn, 5.6°C (10°F) should be added to the measured WBGT for easy work (250 W) and 11.1°C (20°F) should be added for moderate (425 W) or hard (600 W) work.

Frequent measurements of WBGT throughout the day are needed to support this activity; however, measurements of WBGT require specialized, expensive instrumentation as well as experienced operators to obtain accurate, repeatable values. This requirement is particularly true for outdoor measurements, which require careful, time-consuming attention to ensure that reliable data is obtained. Because of the difficulty involved in measuring the WBGT, it would be helpful to be able to predict it from local meteorological measurements, providing the WBGT model had sufficient accuracy. Each of the storage depots has an array of towers that provide continuous meteorological data, which could be used to provide input to a WBGT model. As Table I shows, the U.S. Army work/rest guidelines include five heat categories. Each heat category spans a range of 1.1–1.7°C (2–3°F). The work/rest regimens in the OSHA guidelines span similar ranges. Therefore, to identify the correct heat category, a WBGT model must be accurate to better than 1°C.

To permit continuous monitoring of the working environment, efforts have been made to model the WBGT for indoor[3–6] and outdoor[7] situations using measurements that are more easily obtained. Although valuable for industrial situations, the indoor models do not account for time-varying incident and reflected solar irradiance or for time-varying thermal radiation from the atmosphere and ground surface. The outdoor WBGT model of Hunter and Minyard[7] uses a regression for the natural wet bulb temperature—the predominant component of the WBGT, which they derived from local meteorological measurements. Such an empirical approach can work well locally; however, its application is limited to the location and range of conditions for which it was developed.

In its *Criteria for a Recommended Standard on Occupational Exposure to Hot Environments*,[8] the National Institute

TABLE I. U.S. Army Work/Rest Guidelines

Heat Category	WBGT Index (°C)	Easy Work[A] (250 W)	Moderate Work[A] (425 W)	Hard Work[A] (600 W)
1	25.6–27.7	No Limit (NL)	NL	40/20 min
2	27.8–29.3	NL	50/10 min	30/30 min
3	29.4–31.0	NL	40/20 min	30/30 min
4	31.1–32.2	NL	30/30 min	20/40 min
5	>32.2	50/10 min	20/40 min	10/50 min

Note: Guidelines adapted from Table 3-1 in Ref. 2. Applies to average size and heat-acclimatized soldier wearing battle dress uniform, hot weather.
[A]If wearing nuclear-biological-chemical (NBC) clothing (mission-oriented protective posture (MOPP) level 4), add 5.6°C to WBGT index for easy work and 11.1°C to WBGT index for moderate and hard work.

for Occupational Safety and Health (NIOSH) includes a methodology developed by Mutchler et al.[9] for predicting the WBGT using National Weather Service (NWS) data or local meteorological measurements. The method of Mutchler et al. is based on the regression of locally measured WBGT values against nearby NWS data and local meteorological measurements; for 15 industrial sites, they achieved an average error of 2.4°C. To apply this method, local measurements must first be obtained to generate regression coefficients suitable for the site.

To achieve an accuracy of 1°C or better, independent of location, we have developed a new model of WBGT that is based on fundamental principles of heat and mass transfer and relies only on standard meteorological data. This article describes our WBGT model and its validation using meteorological data and WBGT measurements from the storage depots.

METHODS

The (outdoor) WBGT is the weighted sum of the natural wet bulb temperature T_w, the globe temperature T_g, and the dry bulb (ambient) temperature T_a:

$$\mathrm{WBGT} = 0.7T_w + 0.2T_g + 0.1T_a. \quad \textbf{(1)}$$

Separate models for the natural wet bulb temperature and the globe temperature are necessary to accurately model the WBGT.

Natural Wet Bulb Temperature Model

The psychrometric or aspirated wet bulb temperature and the natural wet bulb temperature are both measured by using a temperature sensor fitted with a wetted wick. In the psychrometric wet bulb measurement, the sensor is typically enclosed in an aspirated radiation shield (e.g., the Assman psychrometer) to isolate the evaporative cooling process. In the natural wet bulb measurement, the wick is completely exposed to the environment, as shown in Figure 1, allowing solar and thermal radiative heat transfer and variable convective heat transfer (as the wind speed varies) to influence the measured temperature. In this way, the natural wet bulb temperature serves as a proxy for the influence of these processes on the human body's ability to cool itself through perspiration.

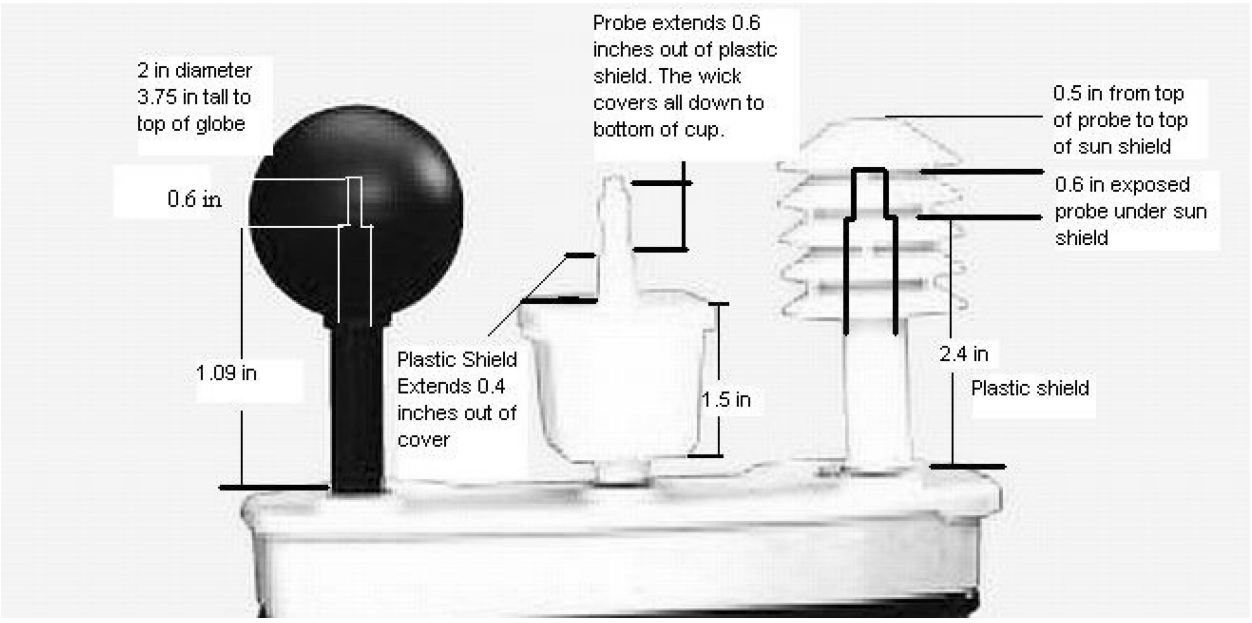

FIGURE 1. An illustration showing the orientation and dimensions of the sensors on the QUEST model QUESTemp°34 WBGT monitor. Note the white surfaces presented to the globe and wick; these are believed to affect the value for the surface albedo derived from the data.

We begin with the psychrometric wet bulb temperature, which is solved as an example in many engineering textbooks on heat and mass transfer,[10,11] as the basis for our model development and add the effects of solar and thermal radiation to the energy balance equation. For either the psychometric or natural wet bulb temperature, the mass balance equation for the wick is

$$\omega\,(1 - x_w) = k_x A\,(x_w - x_a)\,, \tag{2}$$

where ω is the molar water vapor flux from the wick to the air, x_w is the mole fraction of water vapor in the air at the surface of the wick, x_a is the ambient mole fraction of water vapor (i.e., far from the wick), k_x is the convective mass transfer coefficient, and A is the surface area of the wick, which we take to be the surface area of a cylinder of diameter D and length L, such that $A = \pi DL$. For our WBGT instrument, $D = 7$ mm and $L = 25.4$ mm. We neglect the area of the top of the wick because the area ratio $D/4L \ll 1$. The term on the left of the equal sign represents the loss of water by the wick through evaporation, whereas the term on the right represents the corresponding uptake of water vapor by the air.

Using the ideal gas law, the mole fraction can be expressed as

$$x = \frac{n_{\text{vapor}}}{n_{\text{total}}} = \frac{e}{P}, \tag{3}$$

where n is the number of moles, e is the partial pressure of water vapor, and P is the barometric pressure. The partial pressure of water vapor is obtained by using the relative humidity RH (expressed as a fraction of saturation [i.e., between zero and one]) and the saturation vapor pressure e_{sat} at temperature T calculated using the algorithm of Buck.[12] Assuming saturation conditions at the surface of the wick, $e_w = e_{sat}(T_w)$ and $e_a = RH\ e_{sat}(T_a)$. Substituting Eq. 3 back into Eq. 2 and solving for ω yields

$$\omega = k_x A \left(\frac{e_w - e_a}{P - e_w}\right). \tag{4}$$

The energy balance equation for the wick is given by

$$\omega M_{H2O} \Delta H = hA(T_a - T_w) + \Delta F_{net} \tag{5}$$

where ω is the molar vapor flux from the wick to the air as before, M_{H2O} is the molecular weight of water vapor, ΔH is the heat of vaporization, h is the convective heat transfer coefficient, T_a is the ambient temperature, T_w is the temperature of the wick, and ΔF_{net} is the net radiant heat flux from the environment to the wick. (For the psychrometric wet bulb temperature, $\Delta F_{net} = 0$.) The term on the left of the equal sign represents the energy lost by the wick due to evaporation; the terms on the right side of the equal sign represent the energy gained by the wick due to convection and radiation. Equations 2 and 5 can be expressed in terms of the molar vapor flux, combined, and solved for T_w:

$$T_w = T_a - \frac{k_x\ \Delta H\ M_{H2O}}{h}\left(\frac{e_w - e_a}{P - e_w}\right) + \frac{\Delta F_{net}}{A\ h}. \tag{6}$$

The ratio k_x / h can be determined from the analogy between heat and mass transfer:[13]

$$j_H = j_D, \tag{7}$$

where $j_H \equiv \text{Nu Re}^{-1} \text{Pr}^{a-1}$ and $j_D \equiv \text{Sh Re}^{-1} \text{Sc}^{a-1}$ are the Chilton-Colburn j-factors[11] for heat and mass transfer, respectively. The Nusselt number $\text{Nu} = hD/k$, where h is the convective heat transfer coefficient, D is the diameter of the cylinder, and k is the thermal conductivity of the fluid (i.e., air in the present case). The Reynolds number is $\text{Re} = \rho VD/\mu$, where ρ is the fluid density, V is the fluid velocity, D is the diameter of the cylinder, and μ is the fluid viscosity. The Prandtl number is $\text{Pr} = c_p\mu/k$, where c_p is the specific heat at constant pressure. The Sherwood number is the mass transfer analog of the Nusselt number: $\text{Sh} = k_x MD/(\rho\mathcal{D})$, where k_x is the convective mass transfer coefficient, M is the average molecular weight of the fluid (dry air), and $\mathcal{D}$ is the diffusivity (of water vapor in air). The Schmidt number is the mass transfer analog of the Prandtl number: $\text{Sc} = \mu/(\rho\mathcal{D})$. Equation 7 can be solved for k_x / h to yield

$$\frac{k_x}{h} = \frac{1}{c_p M_{Air}}\left(\frac{\text{Pr}}{Sc}\right)^a \tag{8}$$

and substituted back into Eq. 6

$$T_w = T_a - \frac{\Delta H}{c_p}\frac{M_{H2O}}{M_{Air}}\left(\frac{\text{Pr}}{Sc}\right)^a\left(\frac{e_w - e_a}{P - e_w}\right) + \frac{\Delta F_{net}}{A\ h}. \tag{9}$$

The convective heat transfer coefficient in the term $\Delta F_{net}/Ah$ in Eq. 9 is obtained from the dimensionless, empirical correlation for heat or mass transfer from a cylinder in cross flow given by Bedingfield and Drew:[14]

$$\text{Nu Re}^{-1} \text{Pr}^{a-1} = b\,Re^{-c} \tag{10}$$

where $a = 0.56, b = 0.281$, and $c = 0.4$. Solving for the convective heat transfer coefficient yields $h = k/D\ b\ \text{Re}^{1-c}\ \text{Pr}^{1-a}$. Equation 9 shows that the natural wet bulb temperature depends on wind speed through the Reynolds number in the correlation for the convective heat transfer coefficient in the term $\Delta F_{net}/Ah$. As mentioned earlier, for $\Delta F_{net} = 0$, Eq. 9 reduces to the psychrometric wet bulb temperature T_{psy}, which is independent of wind speed because the term $\Delta F_{net}/Ah$ vanishes.

The net radiative gain by the wick from the environment is

$$\begin{aligned}\Delta F_{net} = {} & A\,\sigma\varepsilon_w\frac{1}{2}\left(\varepsilon_a T_a^4 + \varepsilon_{sfc} T_{sfc}^4\right) - A\sigma\varepsilon_w T_w^4 \\ & + A_1(1 - \alpha_w)(1 - f_{dir})S \\ & + A_2(1 - \alpha_w) f_{dir} S/\cos(\theta) \\ & + A\,(1 - \alpha_w)\alpha_{sfc} S.\end{aligned} \tag{11}$$

The first term on the right of the equal sign represents the thermal radiation emitted by the atmosphere and ground surface that is absorbed by the wick, where σ is the Stefan-Boltzmann constant; ε_w, ε_a, and ε_{sfc} are, respectively, the emissivity of the wick, atmosphere, and surface; and T_a and

T_{sfc} are, respectively, the temperature of the air and the surface. The second term represents the thermal radiation emitted by the wick. The third and fourth terms represent, respectively, the diffuse and direct solar irradiance absorbed by the wick, where A_1 and A_2 are the areas of the wick involved in the radiation transfer; α_w is the albedo (the ratio of the reflected and incident solar irradiance) of the wick; f_{dir} is the fraction of the total horizontal solar irradiance S due to the direct beam of the sun; $(1-f_{dir})$ is the fraction due to diffuse solar irradiance (i.e., scattered by the atmospheric gases, aerosols, and clouds); and θ is the solar zenith angle. The final term represents the component of the solar irradiance reflected by the surface and absorbed by the wick, where α_{sfc} is the surface albedo.

The area of the wick for diffuse solar irradiance is the sum of the surface area of the side and top of the cylinder, $A_1 = \pi DL + \pi D^2/4 = \mathrm{A}[1 + {}^{D}/_{4L}]$; the area of the wick for the direct solar irradiance is the projection of A_1 normal to the solar zenith angle: $A_2 = DL\sin(\theta) + \pi D^2/4\cos(\theta)$. The area of the top of the wick is neglected for the thermal radiation terms because the ratio $D/4L \ll 1$; however, it is included for the direct irradiance because $A_2 \to \pi D^2/4$ as $\theta \to 0$ (i.e., near solar noon). The area of the top is also included in the effective area for diffuse solar radiation to ensure that the direct and diffuse solar irradiance components sum correctly.

The broadband emissivity of the atmosphere for thermal radiation can be represented as a function of the partial pressure of water vapor:[15] $\varepsilon_a = 0.575e_a^{0.143}$ because water vapor is the dominant absorber in the thermal infrared.

We do not have measurements of the ground surface temperature, nor do we know the ground surface emissivity, which is likely to be close to unity but may vary according to vegetation type, time of year, and soil moisture. Therefore, it is assumed that the effective radiating temperature of the ground surface is equal to the air temperature, that is, $T_{sfc,eff}^4 = \varepsilon_{sfc}\, T_{sfc}^4 = T_a^4$. The validity of this approximation is confirmed later when, for nighttime conditions, $T_w \approx T_{psy}$, which implies $\Delta F_{net} \approx 0$ as expected from Eq. 9. With this approximation Eq. 11 becomes

$$\frac{\Delta F_{net}}{A} = \sigma\varepsilon_w\left[\frac{1}{2}(1+\varepsilon_a)T_a^4 - T_w^4\right] + (1-\alpha_w)S\left[(1-f_{dir})\left(1+\frac{D}{4L}\right) + f_{dir}\left(\frac{\tan(\theta)}{\pi}+\frac{D}{4L}\right)+\alpha_{sfc}\right]. \quad \textbf{(12)}$$

Because $\tan(90^\circ) = \infty$, we set $f_{dir} = 0$ for $\theta \geq 89.5^\circ$ (i.e., if the sun is not fully above the horizon). In addition, $\varepsilon_w = 0.95$, $\alpha_w = 0.4$, and $\alpha_{sfc} = 0.45$, which were derived from comparisons of a subset of nighttime (for ε_w) and daytime (for α_w and α_{sfc}) WBGT data with model calculations. These values were not changed during subsequent comparisons with measurements.

The derived value for α_{sfc} is significantly higher than expected and does not vary from one location to another. It appears that the value for α_{sfc} is influenced by the white surfaces of the WBGT instrument on which the globe, natural wet bulb, and dry bulb sensors are mounted, as shown in Figure 1. This circumstance may cause the model-predicted value of WBGT to differ from the value measured by other WBGT instruments that receive unobstructed ground surface radiation, in which case a different value of α_{sfc} may be appropriate.

In contrast to Hunter and Minyard[7] who fix $f_{dir} = 0.67$, the solar irradiance is partitioned into direct and diffuse components according to

$$f_{dir} = \begin{cases} \exp(3 - 1.34S^* - 1.65/S^*) & \theta \leq 89.5^\circ \\ 0, & \theta > 89.5^\circ, \end{cases} \quad \textbf{(13)}$$

where $S^* = S/S_{max}$; S_{max} is the maximum solar irradiance that would be received in the absence of the atmosphere:

$$S_{\max} = S_0\cos(\theta)/d^2, \quad \theta \leq 89.5^\circ; \quad \textbf{(14)}$$

S_0 is the solar constant ($= 1367$ W/m^2); θ is the solar zenith angle; and d is the earth-sun distance in Astronomical Units (e.g., the mean earth-sun distance $= 1$ A.U.). Algorithms for calculating θ and d from time, latitude, and longitude are readily available.[16]

The coefficients in Eq. 13 were derived by using a year of direct and diffuse solar irradiance data from the Atmospheric Radiation Measurement Program[17] research facility in north central Oklahoma. The data include clear and cloudy sky conditions as well as periods of verdant and senescent vegetation and snow. The data and Eq. 13 are plotted in Figure 2.

T_w is solved for iteratively. Using the dew point temperature as a first guess for T_w, Eqs. 12 and 9 are evaluated to provide a new estimate of T_w. The strongly nonlinear character of

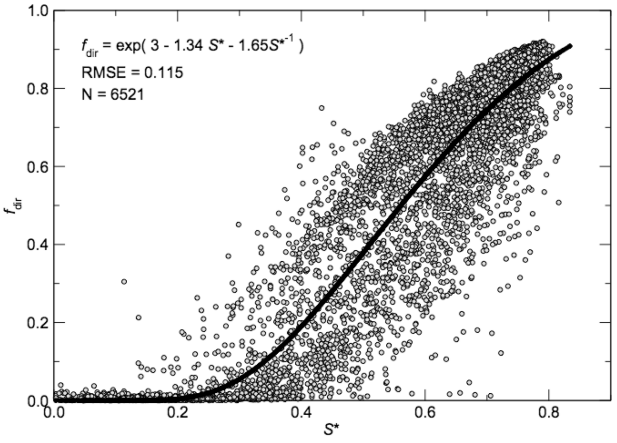

FIGURE 2. The ratio of the direct horizontal solar irradiance to the total horizontal solar irradiance, f_{dir}, as a function of the ratio of the total horizontal solar irradiance to the maximum possible solar irradiance, S^*. Experimental data (open circles) were obtained from the Atmospheric Radiation Measurement Program research facility in north central Oklahoma (36.61°N, 97.49°W). The functional form (solid line) fitted to the 6521 data points has an RMSE of 0.115.

Eq. 12 and the nonlinear dependence of the saturation vapor pressure on temperature requires a relaxation approach: the value of T_w used in the next iteration is the weighted sum of the new estimate and the input to the prior iteration: $T_{w,\,\text{next}} = 0.1\ T_{w,\,\text{new}} + 0.9\ T_{w,\,\text{previous}}$. All properties are evaluated prior to each iteration at the average of the wick temperature and the air temperature. The iteration is stopped when $| T_{w,\,\text{new}} - T_{w,\,\text{previous}} | < 0.02^{\circ}\text{C}$.

Because the natural wet bulb temperature contributes 70% to the WBGT, the accuracy of the model for the natural wet bulb temperature is critical. By setting $\Delta F_{net} = 0$, the psychrometric wet bulb temperatures computed at 101.325 kPa (sea level), 92.6 kPa (750 m above sea level), and 84.6 kPa (1,500 m above sea level) has been verified to agree with published psychrometric charts.[18]

Globe Temperature Model

The globe temperature is measured using a hollow metal sphere, painted black and fitted with an internal temperature sensor. It is fully exposed to the time-varying radiative and convective heat transfer processes in the environment and serves as a proxy for the effect of these processes on the human body.

The energy balance equation for the globe is

$$\begin{aligned} A\varepsilon_g\sigma T_g^4 + Ah(T_g - T_a) = {} & \frac{A}{2}\varepsilon_g\sigma\left(\varepsilon_a T_a^4 + \varepsilon_{sfc} T_{sfc}^4\right) \\ & + \frac{A}{2}(1-\alpha_g)(1-f_{dir})S \\ & + \frac{A}{4}(1-\alpha_g) f_{dir} S/\cos(\theta) \\ & + \frac{A}{2}(1-\alpha_g)\alpha_{sfc} S. \end{aligned} \qquad \textbf{(15)}$$

The two terms on the left of the equal sign represent the energy lost by the globe due to thermal radiation and convection, respectively. $A = \pi D^2$, the surface area of a sphere of diameter D; ε_g is the globe emissivity. $D = 50.8$ mm for our WBGT instrument. The convective heat transfer coefficient is determined by using the empirical correlation for heat transfer from a sphere:[8]

$$\text{Nu} = 2.0 + 0.6\ \text{Re}^{1/2}\,\text{Pr}^{1/3}; \quad h = k/D\ \text{Nu}. \qquad \textbf{(16)}$$

The first term on the right side of the equal sign in Eq. 15 is the energy gained by the globe due to thermal radiation from the atmosphere and surface. As above, we substitute $\varepsilon_{sfc} T_{sfc}^4 = T_a^4$. The second and third terms on the right represent the energy gained by the globe due to diffuse and direct solar irradiance. It is important to note that these act on different areas: the diffuse irradiance is incident on the upper hemisphere of the globe, whereas the direct irradiance is incident on the projected area of the globe normal to the solar zenith angle, which is the cross-sectional area of the globe, $\pi D^2/4$. The final term on the right represents the solar irradiance reflected from the surface that is absorbed by the globe. Equation 15 may now be rearranged as follows:

$$\begin{aligned} T_g^4 = {} & \frac{1}{2}(1+\varepsilon_a)T_a^4 - \frac{h}{\varepsilon_g\sigma}(T_g - T_a) \\ & + \frac{S}{2\varepsilon_g\sigma}(1-\alpha_g)\left[1 + \left(\frac{1}{2\cos(\theta)} - 1\right) f_{dir} + \alpha_{sfc}\right]. \end{aligned} \qquad \textbf{(17)}$$

We set $\varepsilon_g = 0.95$, $\alpha_g = 0.05$, and $\alpha_{sfc} = 0.45$ as before based on comparisons of a subset of the nighttime and daytime WBGT data with model calculations.

Equation 17 is solved for T_g using an iterative, relaxation solution similar to that described above for T_w except that the air temperature is used for T_g on the first iteration. Properties are evaluated prior to each iteration at the average of the globe temperature and air temperature.

WBGT Measurements

The QUESTemp°34 portable heat stress monitor (QUEST Technologies, Oconomowoc, Wis.) was used to acquire WBGT data for model validation. As shown in Figure 1, the instrument has a 50.8 mm diameter globe temperature sensor. A natural wet bulb temperature sensor that is 25.4 mm high is mounted on top of a small water reservoir. The dry bulb air temperature sensor is enclosed in a naturally ventilated radiation shield. According to the manufacturer, the accuracy of the QUESTemp°34 measurements of natural wet bulb, globe, and dry bulb temperature is ± 0.5°C. Our experience suggests the QUESTemp°34 measurements may be better than this. During side-by-side laboratory operation two QUESTemp°34 instruments produced identical values; comparison of the (dry bulb) air temperature sensor with a laboratory reference thermometer revealed a bias of 0.1°C.

We sought to obtain measurements during high-temperature summer periods when heat stress is of greatest concern. Data acquisition periods were normally two continuous days or about 48 hours. At each depot, one QUESTemp°34 instrument was either mounted at the 2-m level of the primary meteorological tower or mounted on a separate 2-m tripod deployed in proximity to the primary meteorological tower and on the south side to ensure that the tower would not shade the instrument. The WBGT instrument was oriented so as to minimize the possibility of one sensor shading the other or obstructing airflow from the prevailing wind direction. The wet bulb reservoir was filled with distilled water at ambient temperature. (Water that is significantly warmer or cooler than ambient temperature will act to cause a bias in the natural wet bulb measurement.)

Measurements of T_g, T_w, T_a, and WBGT were recorded by the instrument at 1-min intervals (not 1-min averages), which is the highest sampling rate available for this instrument. After the instrument was recovered from the field, 15-min averages were formed from the 1-min samples to match the 15-min averages (of 1-sec samples) of the data from the meteorological tower. The slow response of the globe and natural wet bulb

TABLE II. Meteorological Instrumentation and Measurement Accuracy

Argonne-Installed Instrumentation		
Anniston Army Depot, Ala.	Tower 1	33.68350°N, 85.96180°W
Bluegrass Army Depot, Ky.	Tower 1	37.73219°N, 84.19316°W
Newport Chemical Depot, Ind.	Tower 1	39.85377°N, 87.41741°W
Pueblo Chemical Depot, Colo.	Tower 2	38.35593°N, 104.33138°W
Umatilla Chemical Depot, Ore.	Tower 4	45.84623°N, 119.41817°W
Measurement	*Accuracy*	*Instrument*
Air Temperature (Dry Bulb)	±0.05°C	YSI 703 Temperature Sensor in Climatronics Aspirated Shield
Relative Humidity	±2%	Vaisala HMP45D Humidity Sensor
Wind Speed	±Max{0.07, 1%} m/s	Climatronics F460 Anemometer
Total Horizontal Solar Irradiance	±5%	Eppley 8-48 Pyranometer
Barometric Pressure	±0.75 mb	Setra 276 Pressure Sensor
BLM-Installed Instrumentation		
Pine Bluff Arsenal, Ark.	Tower 3[A]	34.31911°N, 92.10717°W
Deseret Chemical Depot, Utah	Tower 9	40.2928°N, 112.3692°W
Measurement	*Accuracy*	*Instrument*
Air Temperature (Dry Bulb)	±0.5°C	Handar 432A (435 A at 2 m)
Relative Humidity	±10%	Handar 435A
Wind Speed	±0.25 m/s	R. M. Young 453AQ
Total Horizontal Solar Irradiance	±5%	Li-Cor LI-200 Pyranometer
Barometric Pressure	±0.55 mb	Setra 270 Pressure Sensor

[A]Relative humidity and barometric pressure obtained from 5-m level of Tower 1 and 1 km away (same elevation and ground cover).

temperatures relative to the meteorological variables dictates the slower sampling rate.

For several depots, additional QUESTemp°34 instruments were deployed at one or two other location(s) where personnel would be working outdoors to assess the spatial variation of WBGT measurements.

Meteorological Measurements

Meteorological data is available at each chemical munitions storage depot from a networked array of instrumented towers operated by the Chemical Stockpile Emergency Preparedness Program (CSEPP). The primary tower at each depot provides 15-min averages of 1-sec samples of temperature, barometric pressure, relative humidity, wind speed and direction, solar irradiance, and precipitation. The instrumentation used to obtain these measurements varies, depending on whether the instrumentation on the towers was installed by Argonne National Laboratory (Argonne) or the U.S. Bureau of Land Management (BLM). The instrumentation and their measurement accuracies are summarized in Table II. The instruments are audited at 6-month intervals and recalibrated as needed. The data is closely monitored for quality and is automatically collected and transmitted to a central location at each depot for display and for emergency response purposes.

Two-Meter Wind Speed Estimation

At each depot, temperature and relative humidity measurements are available at the 2-m level, but wind speed and direction measurements are available at the 10-m, 15-m, 30-m, and/or 60-m level(s). At most depots, we have obtained supplemental 2-m wind speed measurements by using the same type of wind speed sensor that is used on the Argonne-installed meteorological towers mounted on the same tripod as the WBGT instrument. This additional data is necessary to provide model input data at the same height as the WBGT measurements. It also permits us to investigate the impact on model performance of using 2-m wind speeds estimated from measurements at higher levels on the tower, as will be necessary for routine computation of WBGT.

A power-law representation of the vertical profile of wind speed[19] is used to estimate the wind speed at a 2-m height: $u_{2m} = u_{10m}\,(z_{2m}/z_{10m})^p$, where u_{10m} is the 10-m wind speed, z_{2m}/z_{10m} is the ratio of the sensor heights, and the exponent p is a function of the atmospheric stability class as shown in Table III for urban and rural settings. The stability class

TABLE III. Power-Law Exponents for Urban and Rural Wind Profiles

Stability Class	Urban Exponent	Rural Exponent
A	0.15	0.07
B	0.15	0.07
C	0.20	0.10
D	0.25	0.15
E	0.30	0.35
F	0.30	0.55

Source: U.S. Environmental Protection Agency, Table 6-2.[19]

indicates whether and how much the ground surface is being radiatively heated (Classes A, B, C), cooled (Classes E, F) or neither (class D). It is calculated during the daytime by using the solar irradiance and the 10-m wind speed.[19] At night the stability class is calculated using the temperature difference between the 10-m and 2-m levels and the wind speed at the 10-m level.[19]

RESULTS

Model validation comprises several facets: validation against a known standard (e.g., the ability to accurately calculate the psychrometric wet bulb temperature discussed above); qualitative accuracy, which is the ability to reproduce theoretically expected behavior, such as for the limiting case of nighttime conditions when $\Delta F_{net} \approx 0$; and quantitative accuracy, or satisfactory agreement with measurements. The qualitative and quantitative accuracy of the natural wet bulb and globe models and measurements are discussed below.

The theory described above provides insight into how the data and the model should behave, which is important for assuring the quality of the data as well as the proper behavior of the model. Nighttime conditions are especially useful for evaluating the data and model. Equation 9 shows that during the daytime when $\Delta F_{net} > 0$, $T_a > T_w > T_{psy}$; however, Eq. 13 shows that at night, when $S = 0$, $^1/_2(1 + \varepsilon_a)T_a^4 \approx T_w^4$ and ΔF_{net} will be nearly zero (slightly positive or negative) such that $T_w \approx T_{psy}$.

Figure 3 presents a comparison from the Blue Grass Army Depot near Richmond, Ky., for which the natural wet bulb temperature from both the model and data are approximately equal to the psychrometric wet bulb temperature at night, as predicted by the theory. Figure 4 presents a similar comparison for the Pueblo Chemical Depot near Pueblo, Colo., where the measured natural wet bulb temperature deviates from the predicted natural wet bulb temperature beginning near noon, reaches a maximum deviation near sunset, and only gradually falls to the psychrometric wet bulb temperature by dawn. The cause of these deviations remains unclear; it may be that the water in the natural wet bulb reservoir becomes heated by prolonged exposure to the sun, thereby elevating the natural wet bulb temperature, which is followed by gradual cooling during the night. Similar behavior has been observed under similar conditions at the Deseret Chemical Depot near Tooele, Utah.

For the globe temperature at night, Eq. 17 suggests that $T_g < T_a$ for light wind conditions when h is small because $^1/_2(1 + \varepsilon_a) < 1$, especially for low humidity conditions when ε_a is low. The modeled and measured values of T_g in both Figures 3 and 4 exhibit this behavior.

Scatter plots of modeled and measured values of T_w, T_g, and WBGT are presented in Figure 5 for the Blue Grass Army Depot. Table IV shows a statistical summary of the comparisons at all depots, which includes the number of samples acquired, the percentage of samples where the magnitude of the difference between predicted and measured WBGT exceeded 1°C, and the mean difference (bias) and root-mean-square difference or

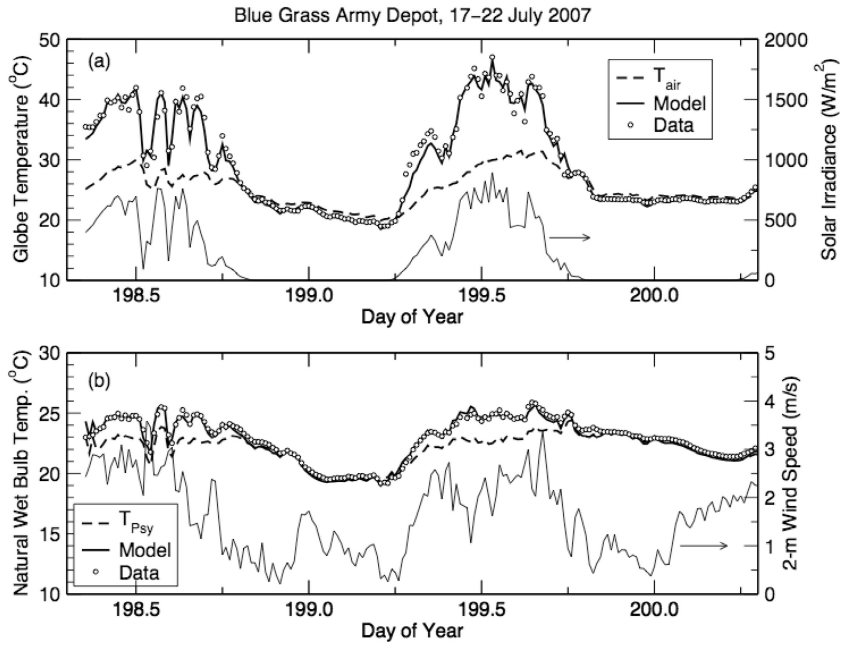

FIGURE 3. Time series plots of (a) the globe temperature from the model (thick solid line) and data (open circles), 2-m air temperature (dashed line), and solar irradiance (thin line); (b) the natural wet bulb temperature from the model (thick solid line) and data (open circles), psychrometric wet bulb temperature (dashed line), and 2-m wind speed (thin line) for the Blue Grass Army Depot near Richmond, Ky.

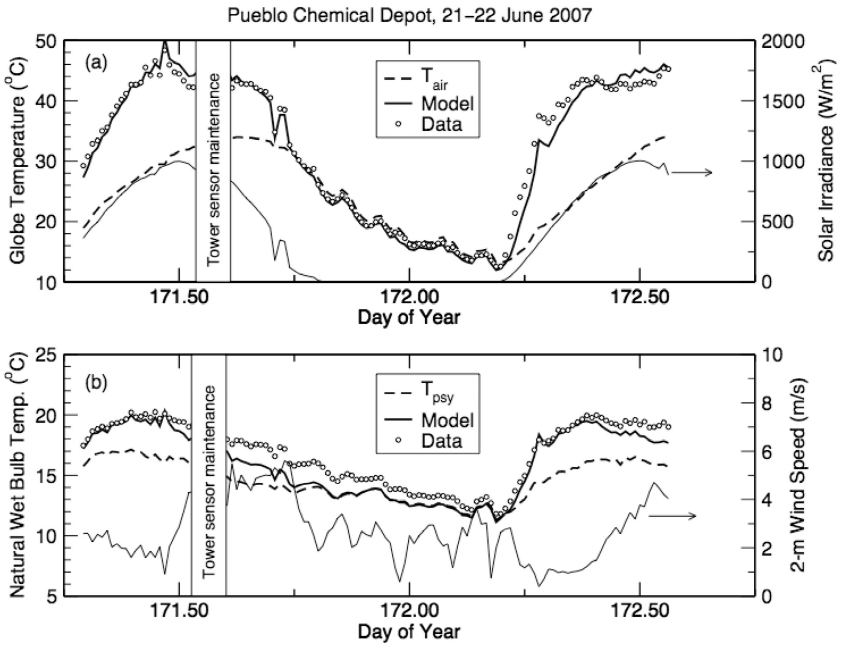

FIGURE 4. Same as Figure 3 but for the Pueblo Chemical Depot near Pueblo, Colo. Tower sensors were lowered for inspection and calibration shortly after noon on Day 171. This circumstance primarily affects the 10-m and 30-m wind speed measurements.

error (RMSE) between predicted and measured WBGT, natural wet bulb temperature, and globe temperature. The results show that for Anniston, Blue Grass, Newport, and Umatilla, the bias is 0.4°C or less, with the bias at Pine Bluff only slightly higher. The 0.7°C bias for Deseret and Pueblo reflects the considerable bias in the natural wet bulb temperature comparison at these depots, which are attributed to problems with the measured wet bulb temperature described above. The RMSE is still less than 1°C despite the relatively large biases because the standard deviation of the differences is comparable to the other depots.

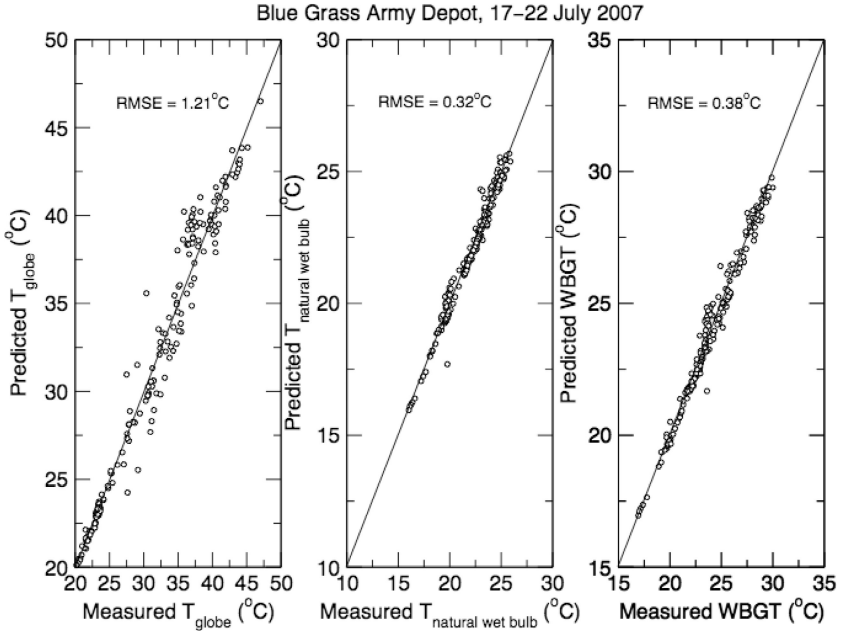

FIGURE 5. Scatter plots of measured and modeled globe temperature, natural wet bulb temperature, and wet bulb globe temperature for the Blue Grass Army Depot near Richmond, Ky. The RMSE between the model and data are indicated on each plot.

TABLE IV. Comparison of Model Predictions with Measurements

Depot	$N_{samples}$	ΔWBGT^A > 1°C	WBGT *Bias (RMSE)*	$T_{natural\ wet\ bulb}$ *Bias (RMSE)*	T_{globe} *Bias (RMSE)*
Anniston, Ala.	180	9%	0.31 (0.57)	0.10 (0.49)	−0.79 (1.76)
Blue Grass, Ky.	219	1%	−0.07 (0.38)	−0.11 (0.32)	−0.09 (1.21)
Deseret, Utah	74	24%	−0.70 (0.90)	−1.08 (1.18)	−0.10 (1.18)
Newport, Ind.	98	3%	0.24 (0.42)	0.10 (0.45)	0.64 (1.43)
Pine Bluff, Ark.	123	14%	0.48 (0.80)	0.28 (0.62)	1.18 (2.04)
Pine Bluff, Ark.^{B}	123	4%	0.15 (0.47)	0.10 (0.48)	0.21 (0.97)
Pueblo, Colo.^{C}	118	30%	−0.73 (0.83)	−0.88 (1.03)	−0.49 (1.63)
Umatilla, Ore.^{C}	95	0%	−0.41 (0.47)	−0.60 (0.61)	−0.12 (0.90)

Note: Bias, RMSE in °C. Bias = predicted – measured.

$RMSE = \sqrt{(Bias)^2 + \frac{N-1}{N}(Std.\ Dev.)^2}$.

^{A}Percentage of cases where the magnitude of the difference between predicted and measured WBGT exceeded 1°C.

^{B}Solar irradiance measurements corrected for ~20% calibration error.

^{C}No 2-m wind speed data available; 2-m wind speeds estimated using 10-m wind speeds.

The percentage of WBGT comparisons exceeding a 1°C difference ranges from 0%–9% except for Deseret, Pueblo, and Pine Bluff. For Deseret and Pueblo, this again reflects the problem with the measured natural wet bulb temperature. At Pine Bluff, the exceedences (and the significant bias in the globe temperature) probably resulted from an error in the calibration of the solar irradiance sensor, which a subsequent audit revealed was reporting ~20% too high. Reducing the measured irradiance by 20% reduced the bias in T_g and WBGT to 0.21°C and 0.15°C, respectively, reduced the RMSE in T_g and WBGT to 0.97°C and 0.47°C, respectively, and reduced the 1°C exceedences to 4%. Also at Pine Bluff, measurements of ambient temperature and relative humidity were not available at the 2-m level on the tower where the WBGT instrument was deployed. These were initially supplied from a tower approximately 1 km away.

However, the temperature from the distant tower exhibited a 1°C bias compared with the dry bulb temperature measured by the WBGT instrument and produced a corresponding bias in the predicted globe and natural wet bulb temperatures when input to the model. The results in Table IV for Pine Bluff reflect the use of the dry bulb temperature from the WBGT instrument as model input. Based on these results, for a new location the bias and RMSE of WBGT would be expected to be no more than about 0.4°C and 0.5°C, respectively, with 95% confidence that the predicted value of WBGT would be within 1°C of the measured value.

A comparison of estimated and measured 2-m wind speeds at the Blue Grass Army Depot during daytime and nighttime periods is presented in Figure 6. The comparison, based on the urban exponents, yields RMS errors in wind speed of 0.19 m/s or 10% of the mean during the day and 0.12 m/s or 12% of the mean at night. The results of the comparison of WBGT model predictions based on the estimated 2-m wind speeds with WBGT measurements are very nearly identical to the results when using the measured 2-m wind speeds for most depots. At Anniston and Newport the RMSE in WBGT increased by about 0.1°C whereas at Pine Bluff it decreased by 0.2°C.

We find that the urban exponents produce more accurate estimates for the depots located in semiwooded areas, whereas the rural exponents are preferable for depots in open, desert areas. Based on these results it appears that we can use the power-law model to estimate the 2-m wind speed without degrading the performance of the WBGT model.

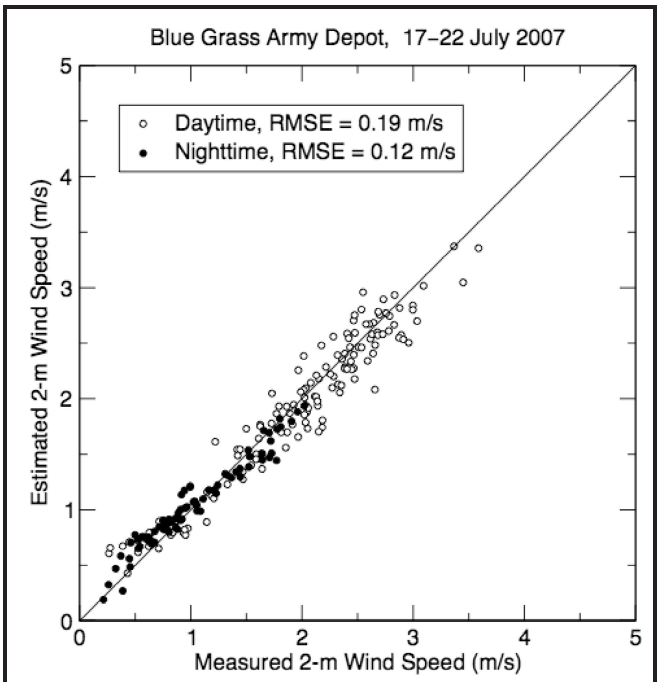

FIGURE 6. Two-meter wind speed estimated using the measured 10-m wind speed and the urban exponents in Table III compared with measured 2-m wind speeds for daytime (open circles) and nighttime (solid circles) periods. The minimum value for the estimated wind speeds is set at 0.13 m/s, the threshold of the wind speed sensors.

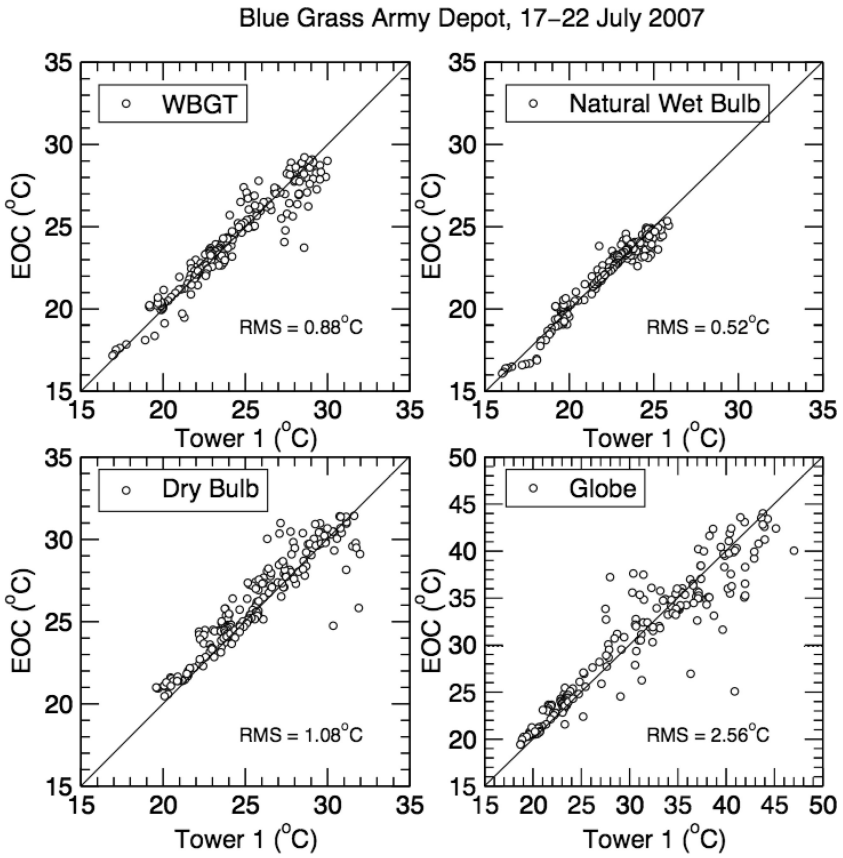

FIGURE 7. Comparisons of WBGT, natural wet bulb temperature, dry bulb temperature, and globe temperature (°C) measured at two locations 7.9 km apart: Tower 1 and the Emergency Operations Center (EOC) at Blue Grass Army Depot. The root-mean-square differences are larger than for the model measurement comparisons in Figure 5.

DISCUSSION

The Argonne model of the WBGT, which has no site-dependent constants (except for the designation of rural or urban exponents for estimating the 2-m wind speed), compares well with measured values of the WBGT and its underlying components when the measurements are accurate. However, there remains an issue of the local spatial variation of WBGT: both the measured and predicted WBGT values represent conditions prevailing at the location of the meteorological tower, which may be a significant distance (e.g., greater than 1 km) from a work site.

To assess the magnitude of the spatial variations of WBGT, measurements were acquired at several locations at the Anniston, Blue Grass, and Pueblo depots. In Figure 7, comparisons of the WBGT and its components from two locations at the Blue Grass Army Depot are presented. The RMS differences for each component are larger than for the model-measurement comparisons, even when using estimated 2-m wind speeds.

The results for Anniston and Pueblo are similar. The largest contributor to the spatial variations in WBGT is the spatial variation in globe temperature, especially on partly cloudy days when one site may be in the sun while another site may be shaded. This result suggests that spatial variations in WBGT may be more significant than uncertainties in the model predictions and that it may be useful to calculate the WBGT using inputs from all towers where solar measurements are available. Nevertheless, the RMS difference between the WBGT measurements is less than 1°C, which would still permit the OHSA or U.S. Army heat categories to be resolved.

CONCLUSIONS

As noted in the NIOSH criteria,[9] predictive models of WBGT are useful for assessing the local heat stress environment and establishing local work practices in advance using forecast (or historical) meteorological values. Accordingly, a model of the WBGT has been developed that relies only on standard meteorological measurements for input. The model is composed of separate submodels for the natural wet bulb temperature and the globe temperature. Because each of these submodels was developed from fundamental heat and mass transfer principles, the models are independent of location and require no local adjustments.

The models have been validated by qualitative and quantitative comparison with WBGT measurements acquired at

seven sites across the United States and spanning a wide range of environmental conditions. At all sites, the RMS difference between the model-calculated WBGT and the measurements was less than 1°C. When the instrumentation was operating correctly the WBGT model predictions exhibited a bias of 0.4°C or less and an RMSE of less than 0.6°C; 91–100% of the WBGT predictions were within 1°C of the measured value. This is true even when using 2-m wind speed values estimated from wind speeds measured at other heights.

Local spatial variations in measured WBGT are shown to be comparable to or greater than the differences between model predictions and measurements. This result suggests it may be useful to calculate WBGT for multiple locations when the necessary meteorological input data are available to achieve maximum accuracy. It also suggests that calculating WBGT may be as useful as measuring WBGT with a device that requires careful, time-consuming attention.

Fortran and C-language programs that implement the Argonne WBGT model are available from the authors.

ACKNOWLEDGMENTS

The authors are grateful to Michael Myirski for insightful comments and suggestions on an early version of the manuscript. This work was sponsored by the U.S. Army Chemical Materials Agency, Chemical Stockpile Emergency Preparedness Program, under Contract MIPR 7D22 CM7007 Amend 01 Rev 12.

REFERENCES

1. **Occupational Safety and Health Administration (OSHA):** Heat stress. In *OSHA Technical Manual*, Chapter 4, Section III (TED 1-0.15A). Washington, D.C.: OSHA, Office of Science and Technology Assessment, 1999.
2. **U.S. Army Center for Health Promotion and Preventive Medicine (USACHPPM):** *Heat Stress Control and Heat Casualty Management* (TB MED 507/AFPAM 48-152). Aberdeen Proving Ground, Md.: USACHPPM, 2003.
3. **Aubertin, M.G.:** Industrial work in a hot environment. In *The Measurement of the Physical Characteristics of a Hot Environment* (Note 1032-85-76). Paris: Institut National de la Recherche Scientifique, 1976. (In French)
4. **Emes, J., S. Mazumdar, C.K. Redmond, P.C. Magee, and E. Kamon:** Models for estimating worksite WBGT. *Am. Ind. Hyg. Assoc. J. 39*:592–597 (1978).
5. **Dernedde, E., and D. Gilbert:** Prediction of wet-bulb globe temperatures in aluminum smelters. *Am. Ind. Hyg. Assoc. J. 52*:120–126 (1991).
6. **Bernard, T.E., and M. Pourmoghani:** Prediction of workplace wet bulb globe temperature. *Appl. Occ. Env. Hyg. 14*:126–134 (1999).
7. **Department of Energy (DOE), Office of Scientific and Technical Information (OSTI):** *Estimating Wet Bulb Globe Temperature Using Standard Meteorological Measurements* by C.H. Hunter and C.O. Minyard (WSRC-MS-99-00757). Oak Ridge, Tenn.: DOE, OSTI, 1999.
8. **Department of Health and Human Services, (DHHS), National Institute for Occupational Safety and Health (NIOSH):** *Criteria for a Recommended Standard —Occupational Exposure to Hot Environments* (DHHS/NIOSH Pub. No. 86-113). Washington, D.C.: DHHS, NIOSH, 1986.
9. **Mutchler, J.E., D.D. Malzahn, J.L. Vecchio, and R.D. Soule:** An improved method of monitoring heat stress levels in the workplace. *Am. Ind. Hyg. Assoc. J. 37*:151–164 (1976).
10. **Bird, R.B., W.E. Stewart, and E.N. Lightfoot:** *Transport Phenomena*. New York: John Wiley & Sons, 1960. pp. 649–652.
11. **Kays, W.M., and M.E. Crawford:** *Convective Heat and Mass Transfer*. New York: McGraw-Hill, 1966. pp. 367–369.
12. **Buck, A.L.:** New equations for computing vapor pressure and enhancement factor. *J. Appl. Meteorol. 20*:1527–1532 (1981).
13. **Chilton, T.H., and A.P. Colburn**: Mass transfer (absorption) coefficients: Prediction from data on heat transfer and fluid friction. *Ind. Eng. Chem. 26*:1183–1187 (1934).
14. **Bedingfield, C.H., and T.B. Drew:** Analogy between heat transfer and mass transfer. *Ind. Eng. Chem. 42*:1164–1173 (1950).
15. **Oke, T.R.:** *Boundary Layer Climates*, 2nd Ed. New York: Methuen & Co., 1978. pp. 373.
16. **U.S. Naval Observatory:** *Astronomical Almanac*. Washington, D.C.: U.S. Government Printing Office, 1985.
17. **Ackerman, T., and G. Stokes:** The atmospheric radiation measurement program. *Physics Today 56*:38–45 (2003).
18. **Perry, R.H., and D.W. Green**: *Perry's Chemical Engineers' Handbook,* 7th ed. New York: McGraw-Hill, 1997. pp. 12-4–12-5.
19. **U.S. Environmental Protection Agency (EPA):** Meteorological data processing. In *Meteorological Monitoring Guidance for Regulatory Modeling Applications* (EPA-454/R-99-005). Washington, D.C.: EPA, 2000.